Nonlinear analysis of thin-walled beams with highly deformable sections

Nonlinear analysis of thin-walled beams with highly deformable sections

E. Carrera[*], A. Pagani[†], D. Giusa[‡], R. Augello[§]

Mul^2 Group
Department of Mechanical and Aerospace Engineering, Politecnico di Torino
Corso Duca degli Abruzzi 24, 10129 Torino, Italy.

Abstract: *This work proposes an alternative approach for the nonlinear analysis of 2D, thin-walled lattice structures. The method makes use of the well-established Carrera Unified Formulation (CUF) for the implementation of high order 1D finite elements, which lay along the thickness direction. In this manner, the accuracy of the mathematical model does not depend on the finite element discretization and can be tuned by increasing the theory approximation order. In fact, the governing equations are invariant of the order of the structural model in CUF. Another advantage is that complex curved geometries can be considered with ease and without altering the nonlinear strain-displacement relations. After a preliminary assessment, attention is focussed on the nonlinear equilibrium analyses of U-shaped 2D lattice structures both in traction and compression. Also, a sensitivity analysis against the effect of various geometrical nonlinear terms is conducted. The results demonstrate the accuracy of the present method, as well as its computationally efficiency, giving confidence for future research in this direction.*

Keywords: Finite element method, Refined 1D theories, Geometric nonlinearities, Large displacements, Lattice structure.

1 Introduction

The need to produce more economical structures is the leading cause of the definition of new theories and optimal design procedures for structures subject to large deformations. A considerable variety of structures can display nonlinear behaviour during their operational life, such as turbine blades, suspended-deck bridge, large-space structures and lattice materials. Given the complex geometry of these structures, ad hoc theories are necessary for a correct nonlinear analysis. The three-dimensional (3D) Finite Element (FE) theories offer high accuracy and a good understanding of the behaviour of the structures in the large-displacements field. However, 3D models can be computationally disadvantageous in a preliminary design

[*]Professor of Aerospace Structures and Aeroelasticity. Corresponding author. E-mail: erasmo.carrera@polito.it

[†]Associate Professor. E-mail: alfonso.pagani@polito.it

[‡]Post Graduate Research Assistant. Email: daniel.giusa@studenti.polito.it

[§]Ph.D. Student. Email: riccardo.augello@polito.it

phase. One-dimensional (1D) theories ensure a considerable reduction in computational cost, and if implemented correctly, they can give accurate results.

The first theories developed were based on the classical models of Euler-Bernoulli [1], Timoshenko [2] and de Saint-Venant [3] in which the 3D structure is reduced to a 1D model whose main variables stands in the beam length axis of the model. Many theories for geometrical nonlinear analysis have been developed starting from the classic theories, and they have received a vivid interest from engineers and researchers. An example is provided in work by Pai and Nayfeh [4], in which special cases of Euler-Bernoulli and Timoshenko theories were developed to deal with the large deflection of composite beams.

Several structures are affected by coupling phenomena (i.e. bending-torsion and axial-bending). In this case, the emplyoment of refined kinematics for the formulation of advanced mathematical models is mandatory. Higher-order theories are also useful in the case an accurate stress analysis is required. Obst and Kapania [5] studied the through-the-thickness shear strain distribution with a geometrical nonlinear beam model accounting only parabolic stress functions. Asymmetric laminated composite beams were analyzed by Singh et al. [6]. They implemented a computational model using the well-known von Kármán nonlinear theory, as well as the 1D FE method. Chandrashekhara and Bangera [7] utilized a higher-order formulation for the shear deformation for flexural analyses of fibre-reinforced composite beams. The Variational Asymptotic Beam Sectional (VABS) is widely used to develop nonlinear analyses in many papers [8]. The three-dimensional case is threated as a combination of a linear part, i.e. the cross-section deformation, and a nonlinear one, i.e. the beam analysis. Krawczyk et al. [9] assumed a shear deformation of a first-order type at the layer level to simulate a partial layer interaction implementing a Layer-Wise (LW) nonlinear beam thoery. The post-buckling behavior of laminated 1D structures were discussed by Emam [10], with the Hamilton's principle approach. The nonlinear problem was solved by developing a beam model based on a three-noded FE by Vidal and Polit [11]. They analyzed the case of laminated beams, and the shear strain distribution was obtained using a sinusoidal interpolation. This approach allowed preventing the adoption of mathematical artifices like shear factors and providing the continuity between adjacent layers. Li and Qiao [12] extended the Reddy's high-order shear deformation beam theory to thermal post-buckling analysis of composite beams, utilizing a kinematics accounting for von Kármán assumptions. The application with initial inclusions and of composite tubular structures was further threated by the same authors in [13, 14]. Mororo et al. [15] recently developed a total Lagrangian approach for the nonlinear study of composite beams with thin-walled sections. An ad-hoc thin-walled beam theory was employed for the calculation of the material matrix of the beams.

The application of beam theories was restricted mainly to slender and solid cross-sectioned beams that do not exhibit complex structure developed in three dimensions, which is evidently not the case of lattice structures. In recent years lattice structures attracted much attention because of their valuable properties. Lattice structures are made of repetitions of unit cells in the three dimensions, and their production has been made much more accessible due to the advancements in additive manufacturing techniques [16]. The main features of lattice structures can be summarized in: (1) reduction of material in the production process, (2) reduction of time in manufacturing, (3) reduction of energy in the production process, (4) high strength/weight optimization [17]. In the case of complex structures, numerous methods have been proposed to take into account beam systems made of 1D elements generally oriented in the 3D space. Lee and Nikolaidis [18] introduced rotational joint springs whose stiffness is measured by the static response of the structure. El-Sayed [19] solved a 3D problem for the joint region to estimate the spring stiffness. Jang et al. [20] proposed a beam connections

theory without any artificial springs. The Guyan reduction was utilized by Donders et al. [21] to develop a FE model of a joint beam elements. The static and modal analyses were investigated [22]. The use of these theories is even more complicated in the case of geometrical nonlinear behaviour, including post-critical behaviour. For this reason, it is necessary to overcome these critical issues and implement a method that deals with complex structures with an immediate and straightforward procedure.

Variable kinematics and refined beam theories can be built conveniently based on Carrera Unified Formulation (CUF) [23, 24]. The CUF methodology was used to analyze the nonlinear behaviors of different structures and there is a considerable number of examples in the literature. Pagani and Carrera [25] introduced CUF for the geometrical nonlinear analysis of metallic thin-walled structure, showing the capabilities of the formulation to deal with large displacements and rotations. The same authors have been extended the CUF formalism to composite laminated beams [26]. Also, using CUF, it has been demonstrated that it is possible to carry out investigations about the consistency of multiple assumptions of the strain measurements in the large displacement and rotation field with ease, see for example [27]. Further examples of CUF applications are the micromechanics analysis [28] hygrothermal [29], thermo-elastic response [30] and [31], and free vibration analysis [32], among the others. Moreover, Carrera et al. [33] have been studied geometrical nonlinear effects over the cross-section of thin-walled/shell-like structure.

The present work illustrates and proposes an alternative procedure, based on CUF, to analyze the large deflection of complex beam structures. Fig. 1a depicts the idea behind and shows a sample one-dimensional (1D) structure, where L is the length, and b and h are the width and the thickness, respectively. In the case of classical beam theories, it is mandatory to choose the beam axis y along the beam length L, as shown in Fig. 1b. The beam axis y lays along the L direction (in blue in the figure), whereas the cross-section Ω_c stays in the $b \times h$ domain (in red). Instead, in case of refined theories, such as CUF one, the y-axis can be placed along any direction, including the width b or the thickness h of the 1D structure. In particular, in the approach presented herein and reported in Fig. 1c, the cross-section Ω_p is in the plane $x - z$ along the directions $L \times h$, and the beam axis y lays along the width direction b. If the Finite Element Method (FEM) is adopted, its discretization is made along the beam axis, which is much shorter in the case of the alternative beam modeling proposed herein. Of course, additional Degrees of Freedom (DoFs) would be necessary for the refinement of the expansion over the $x - z$ plane, which is typical of any refined beam theory. Nevertheless, note that numerical problems related to locking phenomena, which usually afflicts the FEs, such as the shear locking, can be overcome with the proposed alternative model. Finally the nonlinear geometrical relations are simplified, especially in the case of curved structures.

The goal of the present paper is to assess this alternative manner of modeling 1D structures in the case of large displacement analysis of lattice-type structures. In particular, the geometrical nonlinearities, which occur within the structure, are evaluated considering cross-section nonlinearities. In earlier works from Pagani *et al.* [27, 34] and Wu *et al.* [35], various nonlinear theories are addressed to solve the geometrical nonlinear problems of beams and plates, showing how those theories affect the nonlinear static behavior of thin-walled and compact structures in the large displacement and rotations field. The same approach is reported in the present work, considering nonlinearities in the cross-section plane.

This paper is organized as follow: in Section 2, the kinematic relations, the constitutive expressions and the formulation of the refined beam theory (namely CUF and FEM methods) for elastic metallic materials are introduced; in Section 3 the nonlinear governing relations and fundamental nuclei (FN) of secant and tangent matrices are described; numerical results

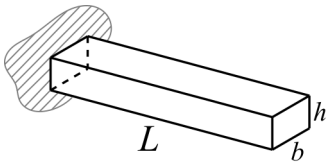

(a) Generic 1D structure

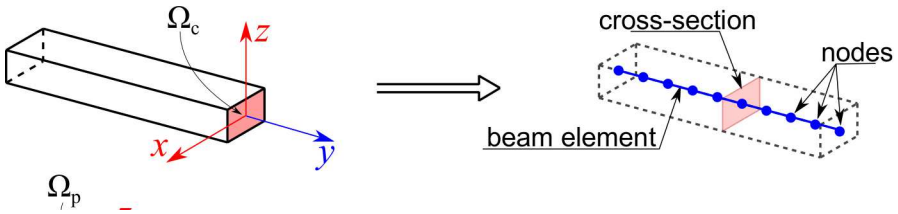

(b) Classical beam formluation: the beam axis "y" is placed along the length "L".

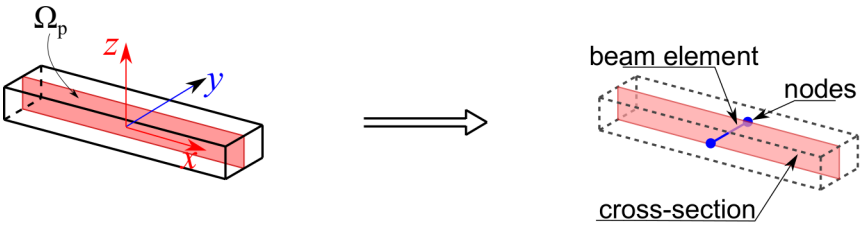

(c) Present alternetive approach: the beam axis "y" is placed along the "b" length.

Figure 1: Comparison with two possible 1D-modeling approaches for a cantilever beam.

are presented in Section 4; finally, the conclusions are discussed in Section 5.

2 Beam models with only displacement unknowns

The three-dimensional (3D) displacement field of a generic one-dimensional (1D) beam structure, as shown in Fig. 1a, can be written in a vectorial form, and it reads:

$$\mathbf{u}(x,y,z) = \left\{ \begin{array}{ccc} u_x & u_y & u_z \end{array} \right\}^T \tag{1}$$

where x, y and z are the coordinates of a Cartesian reference system. Assume that y is the direction of the beam axis, whereas x and z are the coordinates of the cross-section. To clarify this aspect, Fig. 1b reports the classical approach, where the cross-section Ω_c (in red) is the rectangle $b \times h$, and the beam axis (in blue) is placed along the length L direction. On the other hand, the method presented in this work (Fig. 1c) considers the cross-section Ω_p laying in the $L \times h$ domain, and, as a result, the beam axis is along the width b direction. Note that the Cartesian reference system, in both approaches, is placed so that the cross-section lays on the $x - z$ plane and the beam axis in the y direction.
The Carrera Unified Formulation (CUF) and the Finite Element Method (FEM) allow the 3D displacement field to be expressed as follows:

$$\mathbf{u}(x,y,z) = F_\tau(x,z) N_i(y) \mathbf{u}_{\tau i}, \qquad \tau = 1,2,\ldots,M \quad i = 1,2,\ldots,N \tag{2}$$

where $F_\tau(x,z)$ are the cross-section expansion functions in x and z directions, where N_i stands for the i-th shape function in the y direction, M represents the number of the terms used

in the expansion, N stands for the number of the nodes on the beam axis and $\mathbf{q}_{\tau i}$ is the vector of the nodal unknowns. Several cross-sectional functions F_τ can be easily implemented in a unified manner, for further details see Refs. [36, 37]. Here, Lagrange Expansion (LE) is used as cross-sectional function. They can ensure linear (L4), quadratic (L9), and cubic interpolation (L16), allowing the implementation of linear to higher-order kinematics. Carrera and Petrolo [38] provided more details about LE beam theories.
Figure 2 shows how the Lagrange expansion can be used in both conventional and alternative manners of creating beam models for the geometry of Fig. 1a. As the beam deforms over the cross-sections, the alternative manner of modeling the beam leads to the use of only one element along the beam axis. This is not the case of the conventional approach. The use of LE allows clamping the cross-sectional points related to the clamped edge, for example. In addition, shear locking is supposed to be less evident in the alternative procedure proposed herein. Figure 2 shows the classical model and the present approach in which L4 elements are used in both cases to approximate a cantilever beam. For each case, the real structure, the cross-section model with the respective expansion function, the FEM model, and the model subjected to bending deformation are shown. In the figure, a deformation around x axis is supposed. In the classical beam modelling approach (see Fig. 2(a)), important bending/shear stresses and strains are, respectively, calculated by Hooke's law and geometrical relations, which makes use of the derivatives of the shape functions (N_i). As a consequence, scarce FE approximations may bring to numerical issues, such as shear locking. In contrast, by using the method outlined in Fig. 2(b), the shear locking can be attenuated if refined structural theories are used. As a matter of fact, shear strains are computed from the derivatives of higher-order polynomials (F_τ) in this latter case.

The more interesting case of thin-walled beam is shown in Fig. 3. It is clear that nonlinearities along the beam axis of classical beam (the blue domain in the figure) analysis become nonlinearities of the cross-section in the alternative approach discussed herein. Moreover, the latter allows building models of very complex geometries, which would require the adoption of multiple-beam elements and effective methods for their connection with the conventional approach.

3 Brief description of nonlinear CUF based FE model

A compact form of the displacement-strain relations can be obtained by introducing the linear and nonlinear differential operators $\mathbf{b}_l$ and $\mathbf{b}_{nl}$:

$$\epsilon = \epsilon_l + \epsilon_{nl} = (\mathbf{b}_l + \mathbf{b}_{nl})\mathbf{u} \tag{3}$$

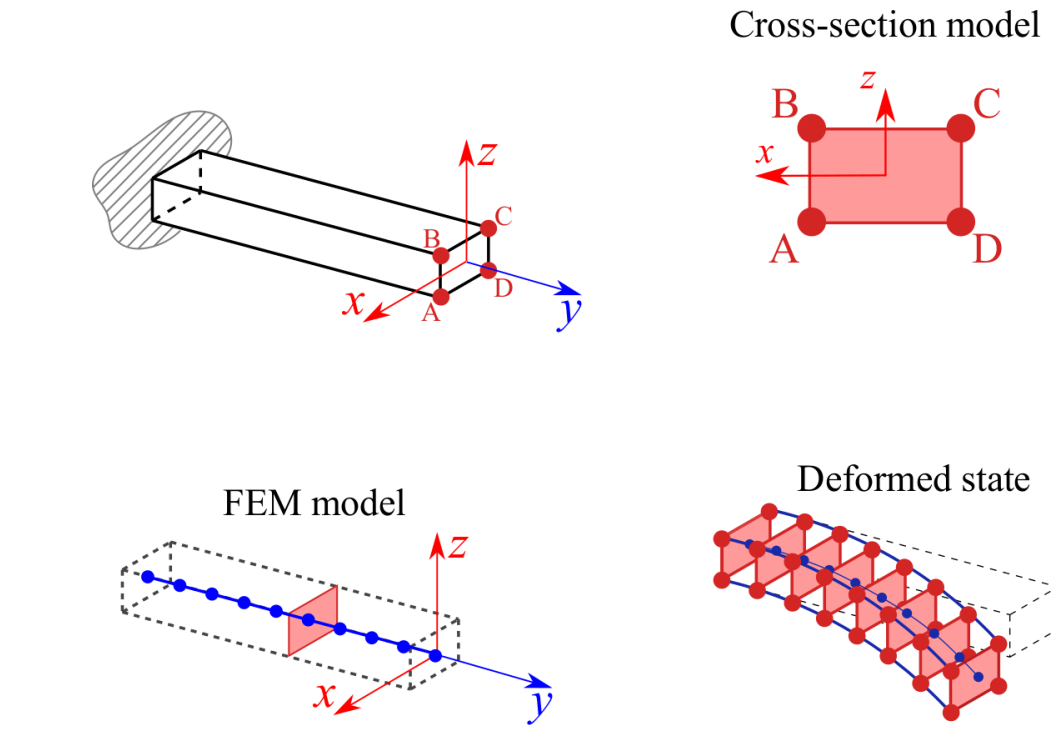

(a) Classical beam model.

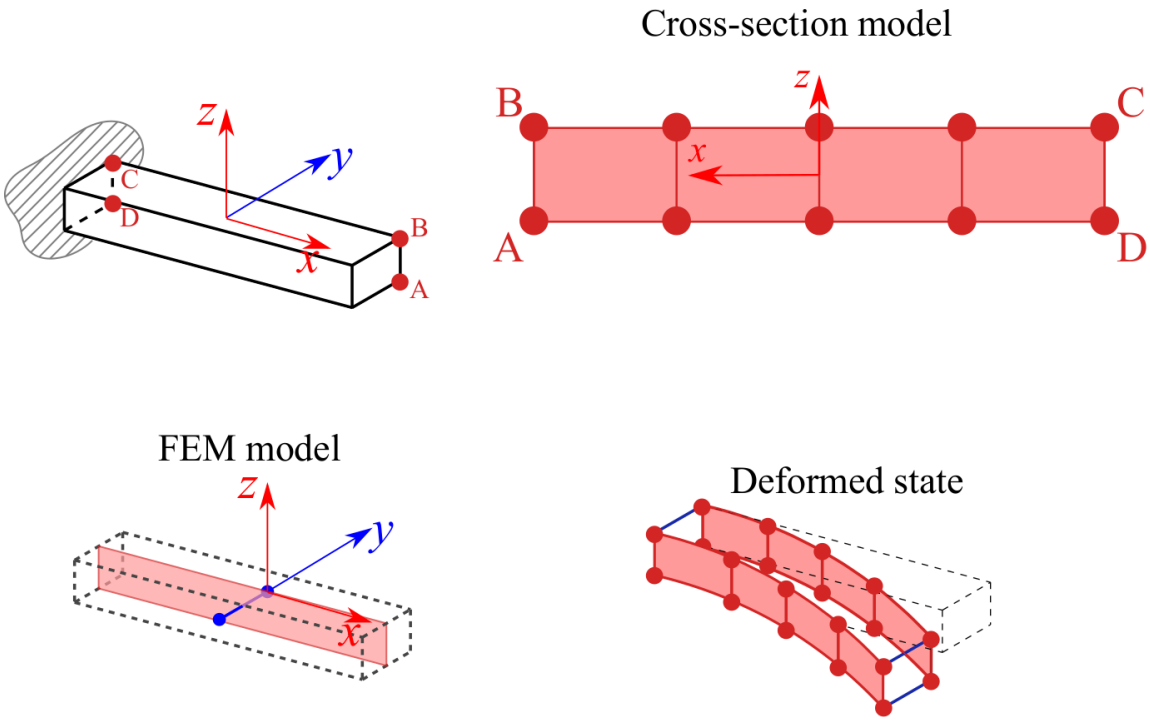

(b) Present beam with large sectional deformation.

Figure 2: Different applications of the CUF-based LE refined beam models.

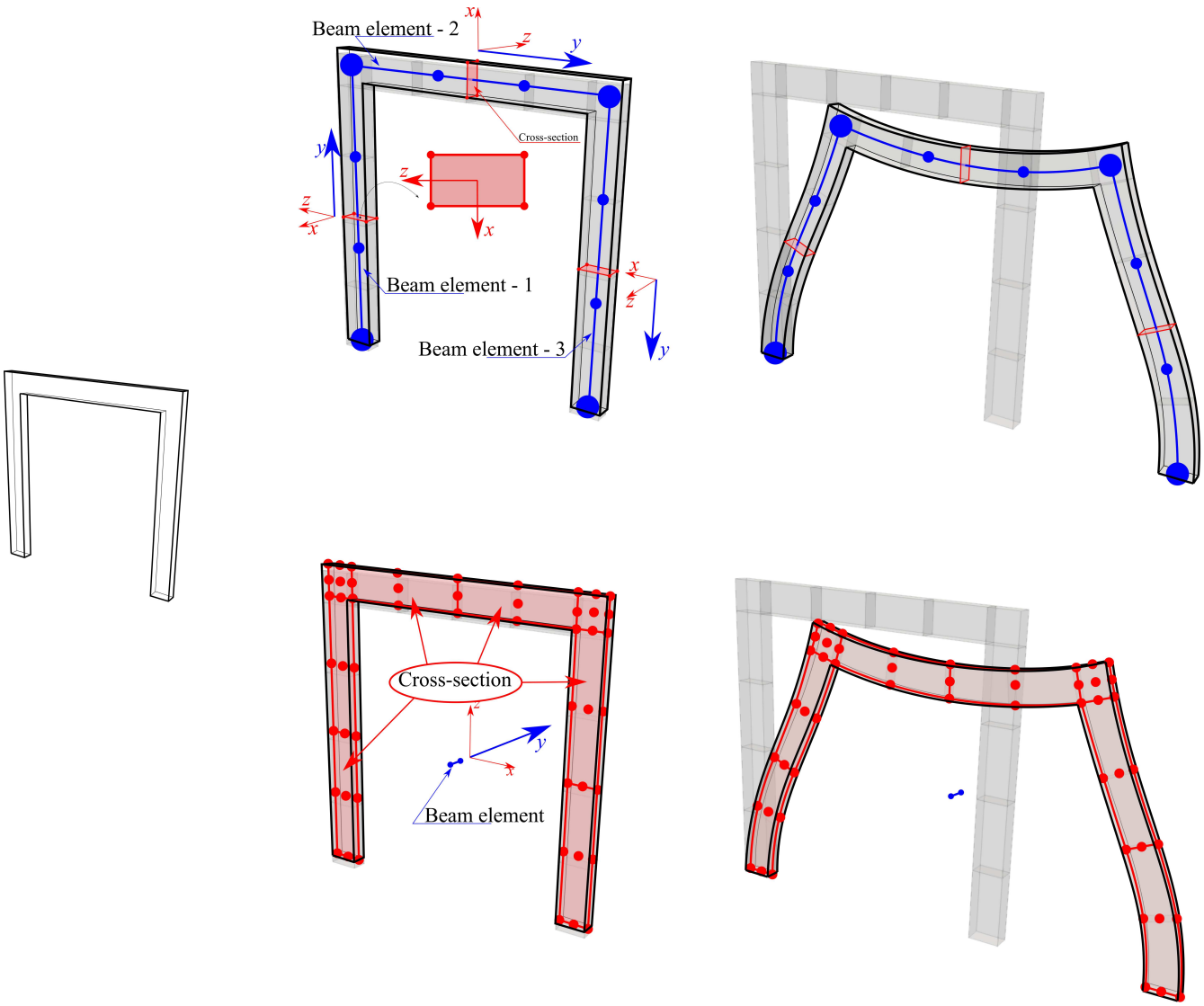

Figure 3: Classical and present approaches for the approximation of a complex thin-walled structure.

where $\epsilon = \{\epsilon_{xx} \quad \epsilon_{yy} \quad \epsilon_{zz} \quad \epsilon_{xz} \quad \epsilon_{yz} \quad \epsilon_{xy}\}^T$ is the strain vector. The complete form of these two matrices is the following:

$$\mathbf{b}_l = \begin{bmatrix} \partial_x & 0 & 0 \\ 0 & \partial_y & 0 \\ 0 & 0 & \partial_z \\ \partial_z & 0 & \partial_x \\ 0 & \partial_z & \partial_y \\ \partial_y & \partial_x & 0 \end{bmatrix}, \qquad \mathbf{b}_{nl} = \begin{bmatrix} \frac{1}{2}(\partial_x)^2 & \frac{1}{2}(\partial_x)^2 & \frac{1}{2}(\partial_x)^2 \\ \frac{1}{2}(\partial_y)^2 & \frac{1}{2}(\partial_y)^2 & \frac{1}{2}(\partial_y)^2 \\ \frac{1}{2}(\partial_z)^2 & \frac{1}{2}(\partial_z)^2 & \frac{1}{2}(\partial_z)^2 \\ \partial_x\,\partial_z & \partial_x\,\partial_z & \partial_x\,\partial_z \\ \partial_y\,\partial_z & \partial_y\,\partial_z & \partial_y\,\partial_z \\ \partial_x\,\partial_y & \partial_x\,\partial_y & \partial_x\,\partial_y \end{bmatrix} \tag{4}$$

The Hooke's law expresses the relation between σ and ϵ for a linear elastic isotropic metallic material, it reads:

$$\boldsymbol{\sigma} = \mathbf{C}\boldsymbol{\epsilon} \tag{5}$$

where $\mathbf{C}$ is the material matrix.It is not given here explicitely, but can be found in [39, 40]). The detailed derivation of the nonlinear problem and the adopted resolution are deeply described in many works, see [25, 33, 41]. For this reason, only the main steps will be described hereafter.

The derivation of the nonlinear finite element governing equations comes from the principle of virtual work. It states that the virtual work from the internal strain energy (δL_{int}) is equal to the one made by the external loads (δL_{ext}). From the variation of the internal strain energy, considering constitutive and geometrical relations, can be expressed as:

$$\begin{aligned} \delta L_{\text{int}} &= \int_V \delta\boldsymbol{\epsilon}^T \boldsymbol{\sigma}\, \mathrm{d}V \\ &= \delta\mathbf{q}_{sj}^T\, \mathbf{K}_S^{ij\tau s}\, \mathbf{q}_{\tau i} \end{aligned} \tag{6}$$

where $\mathbf{K_S}$ represents the so-called secant stiffness matrix. The complete form of the secant stiffness matrix $\mathbf{K}_S^{ij\tau s}$ can be found in [27]. Omitting some mathematical steps, which interested readers can find in [24], after expanding the fundamental nuclei and assembling, the governing equations become:

$$\mathbf{K}_S\, \mathbf{q} - \mathbf{p} = 0 \tag{7}$$

where $\mathbf{K}_S$, $\mathbf{q}$, and $\mathbf{p}$ are the global FE arrays of the structure, with $\mathbf{p}$ corresponding to the loading vector.

Nonlinear algebraic equations are solved via a Newton-Raphson scheme, which requires the linearization of the equations. The related tangent stiffness matrix $\mathbf{K}_T$ can be obtained by the second variation of the strain energy, as follows:

$$\delta^2 L_{\text{int}} = \delta\mathbf{q}_{sj}^T \mathbf{K}_\mathbf{T}^{\mathbf{ij\tau s}} \delta\mathbf{q}_{\tau i} \tag{8}$$

Finally, an arc-length constraint is adopted herein for the system presented in Eq. 8. More detail are presented by Carrera [42] and Crisfield [43, 44].

Back to the geometrical nonlinear relation presented in Eq. (4), it is of particular interest to make evidence of the different meanings of the terms of the matrix $\mathbf{b}_{nl}$, according to the classical and alternative beam formulation considered herein. In fact, one of the significant differences between the two approaches is given by their different behaviour in case of large deformations. Fig. 4a shows the classical models, and in this case, the beam finite element (in blue in the figure) undergoes deformation. Therefore, a substantial number of elements of appropriate accuracy are needed. Instead, the cross-section (in red), if high accuracy is not required, can also be considered non-deformable and classic models can be used to approximate it (e.g. Euler-Bernoulli or Timoshenko beam theories). For the current model, shown in Fig. 4b, it is mandatory to use high-order theories to model the cross-section since the deformation is detected almost exclusively by the cross-section. Instead, the beam finite element undergoes only a translation, and consequently, fewer elements can be used and with less accuracy. This behavior can be addressed by eventually nullifying (white dots Fig. 4a) or adding (black dots Fig. 4a) the nonlinear terms of the full 3D Green–Lagrange strains matrix (Eq. 4). A detailed study of this procedure is presented in Ref. [27]. This simplification of the nonlinear matrix is different according to the type of model used. Obviously, for a classical model, in which the beam elements develop along the main dimension of the structure, the most important parameters are those referred to the y-axis (Fig. 4a). On the other hand, for a model that approximates the geometry of the structure through the cross-section, the terms referring to the x and z directions are much more significant (Fig. 4a).

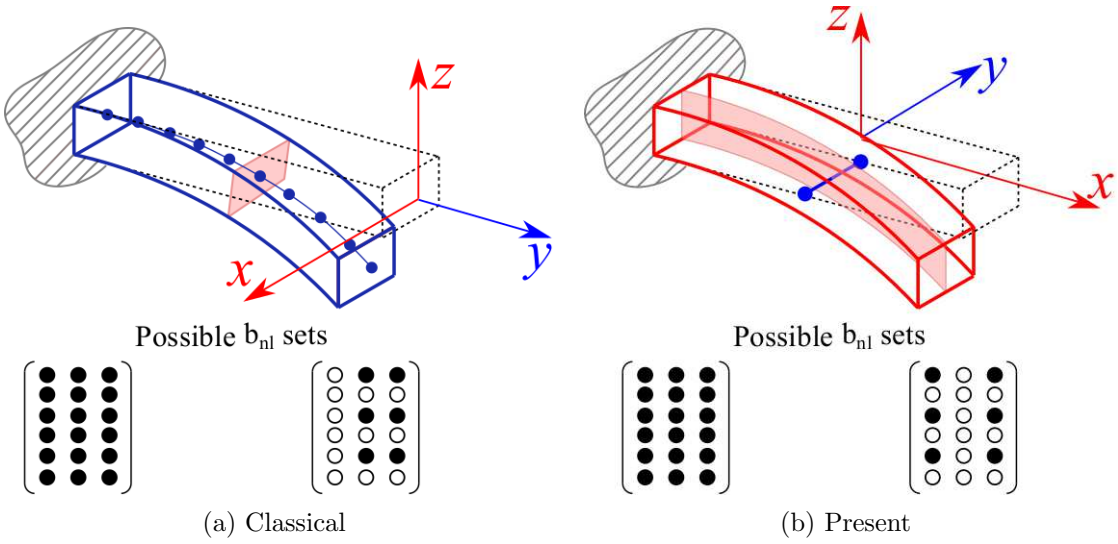

(a) Classical (b) Present

Figure 4: Different modelling approaches demand for different geometrical nonlinear terms.

4 Numerical Results

The effects of section nonlinearities are investigated with practical examples. The unified formulation allows the use of the cross-section expansion function on any side of the structure. In this way, nonlinearities can be treated only on the cross-section. For validation purposes, a reference solution is obtained by comparison with the literature results. The efficiency of the cross-section nonlinear analyses are demonstrated, and the capability of the proposed model to deal with large deflections and post-buckling is highlighted. Then thin-walled structures are considered, with isotopic material and the results are compared to those provided by

commercial software Nastran. Various geometrical nonlinearities are evaluated to identify the essential terms for nonlinear analysis.

4.1 Large deflection and post-buckling of cantilever beams

The post-buckling and large-defletion of a cantilver beam is considered as first analysis case. The structure is made of an aluminum alloy with Young modulus E equal to 75 GPa and Poisson ratio $\nu = 0.33$ and exhibits a square cross-section. The reference solution is taken from Ref. [25], where 20 B4 finite elements and quadratic expansion (L9) are used, as depicted in Fig. 5a. The proposed approach makes use of a different discretization, i.e. the side on the main length of the beam is considered as the cross-section of the model. Quadratic and cubic kinematics are employed in the cross-section, as shown in Fig. 5b. Table 1 shows the normalized vertical displacement at the beam free edge varying the length-to-side ratio and the loading condition. Given the convergence of Table 1, a B3 finite element along with a cubic (10L16) beam theory are used for the subsequent analyses. A similar convergence study has been conducted for the beam treated in Ref. [25]. In this paper, convergence results are found with 20B4 beam elements and a nine-points Lagrange element on the cross-section. Considering the present model with only section nonlinearities, convergence results are obtained with a reduced computational cost. Figure 6a shows the equilibrium curves for a vertical loads and the results of the present beam model are compared to those from linear and nonlinear reference cases. The proposed beam model, taking into account only the section nonlinearities, can describe the large deflections of cantilever beams, in agreement with reference results. The post-buckling behaviour of the same beam structure as considered

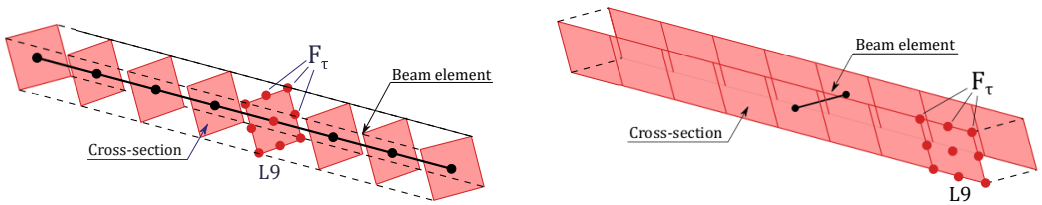

(a) Classical beam element (b) Present beam element

Figure 5: Classical and alternative approaches for the nonlinear analysis of the cantilever square beam subjected to transverse and compression loading conditions.

in the previous analysis case, is addressed. Fig. 6b reports the transverse displacements versus the normalized loading P. Also, in this case, the post-buckling trend is comparable with the reference.

4.2 Thin-walled U-shaped structures

This section aims to investigate the geometrical nonlinear effects of a thin-walled channel-section beam. In Fig. 7 the structure geometry is shown, with w = 0.1 m, h = 0.1 m, and t = 0.01 m. The beam has an elastic modulus equals to 75 GPa and Poisson ratio $\nu = 0.33$. One side of the structure is clamped, while the other is free to move in the x direction. A load, P, is applied in one side of the cross-section, as depicted in figure 7. Along the y axis, the structure is discretized by using a B4 beam element. Three different cross-section discretizations are used to describe the displacement field, and they differ in the number of LE subdomains used to approximate the section. The discretization 8a uses 8 LEs, the discretization 8b

Table 1: Normalized vertical displacement, u_z/L, of the square cross-section cantilever beam for $\frac{PL^2}{EI} = 3$. Reference solution (20B4/1L9) from Ref. [25], $u_z/L = 0.599$ with 1647 DoFs. In brackets, the number of DoFs.

Beam elements	**Cross-section elements**						
Reference	**1L9**			**1L16**			
5B4	$0.594^{(432)}$			$0.594^{(768)}$			
10B4	$0.597^{(837)}$			$0.597^{(1488)}$			
20B4	$0.599^{(1647)}$			$0.599^{(2928)}$			
Present approach	**10L9**	**15L9**	**20L9**	**9L16**	**10L16**	**15L16**	**20L16**
1B2	$0.567^{(378)}$	$0.585^{(558)}$	$0.589^{(738)}$	-	$0.591^{(744)}$	$0.592^{(1104)}$	$0.592^{(1464)}$
1B3	$0.573^{(567)}$	$0.592^{(837)}$	$0.597^{(1107)}$	$0.597^{(1008)}$	$0.599^{(1116)}$	$0.599^{(1656)}$	$0.599^{(2196)}$
1B4	$0.573^{(756)}$	$0.592^{(1116)}$	$0.597^{(1476)}$	-	$0.598^{(1488)}$	$0.599^{(2208)}$	$0.599^{(2928)}$

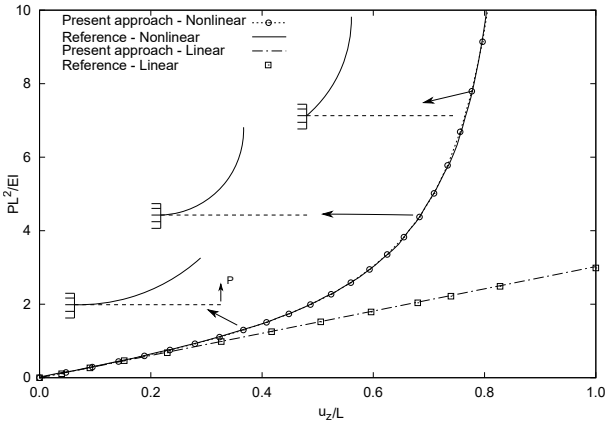

(a) Equilibrium curves of the square cross-section beam subjected to vertical loading. Reference solution from Ref. [25].

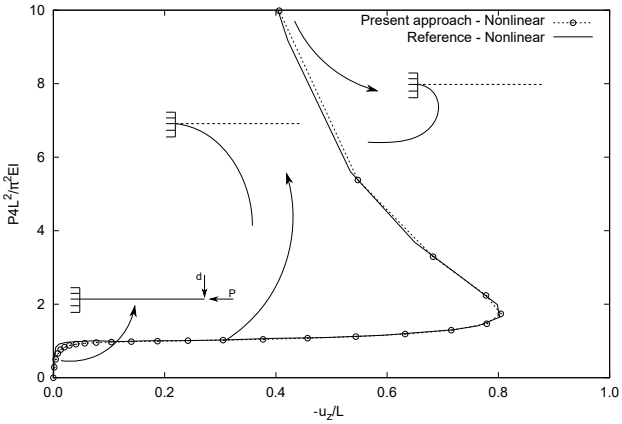

(b) Post-buckling equilibrium curves of the cantilever square cross-section beam. Reference solution from Ref. [25].

Figure 6: Post-buckling of a cantilever square cross-section beam.

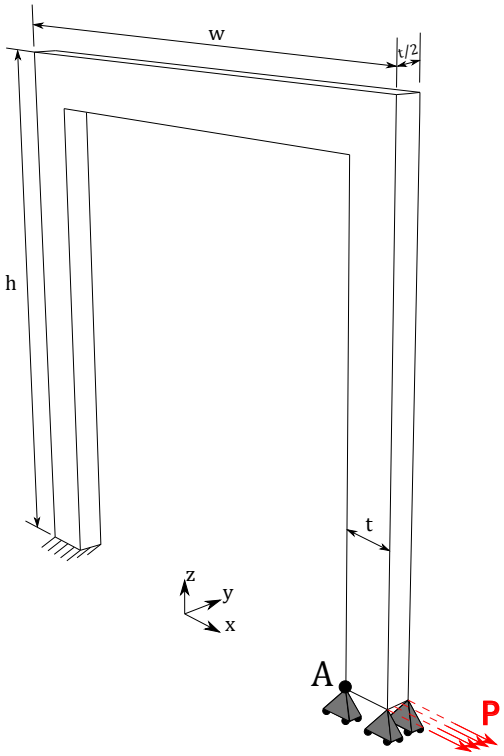

Figure 7: Thin-walled beam geometry and boundary conditions

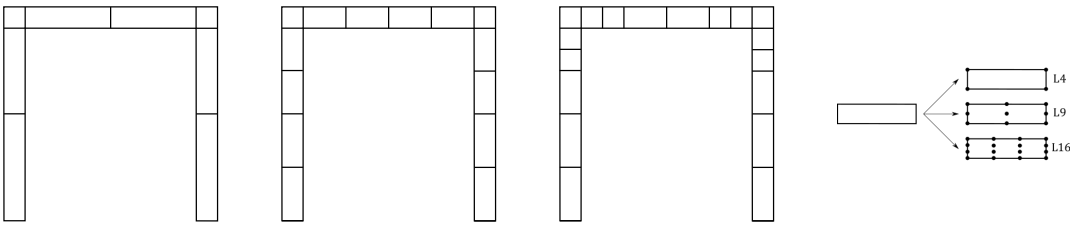

(a) LE model 1 (b) LE model 2 (c) LE model 3 (d) LE polynomials

Figure 8: Different LE models of the thin-walled channel-section structure.

doubles the elements on each side e the discretization 8c, with 18 Lagrane polynomials, is the most refined case. The L4, L9, and L16 LE are adopted for the description of each cross-section, as shown in Fig. 8d. For each discretization and adopted theory, both linear and nonlinear analyses were carried out. The equilibrium curves are shown in Fig. 9a, 10a and 11a, where the displacement of point A is evaluated. In Fig. 9a the equilibrium curves for L4, L9 and L16 elements are plotted for discretization 8a. As predictable, with L4 model, the structure assumes a higher stiffness that leads to lower displacements and the nonlinear trend becomes similar to the linear one. When higher-order theories are employed in the model, the differences between the two static solutions are evident and not negligible. The percentage difference between linear and nonlinear solutions is shown in Fig. 9b. A bilinear description is not accurate, thus the cases with L4 elements have been discarded for subsequent analyses. In Figs. 10a and 11a the L9 and L16 curves are similar for both discretization schemes. Further analyses on computational costs demonstrate that the discretization 8c leads to similar results compared with discretization 8b. Therefore the case 8b offers the best compromise between computational cost, denoted by DoFs, and accuracy. Taking the displacements of the most refined configuration with L16 elements as reference, the percentage errors are evaluated and listed in Table 2. The second discretization with L16 elements leads to negligible error, and the computational saving is evident. The MAPE (Mean Absolute percentage error) provides, in a single value, the accuracy of a configuration compared to the reference one. Finally, the model is analyzed with 3D FEs with the commercial software Nastran. The model has 5095 DoFs. The percentage difference between the CUF and the 3D solutions is negligible, but the proposed approach leads to a considerable computation saving of about 50% of the DoFs.

Table 2: DoFs and errors on displacement of point A, depicted in Fig. 7, considering various model discretization. 3D*: Nastran solution: 1695 HEXA elements.

	Discretization 1		**Discretization 2**		**Discretization 3**		**3D***
P [kN]	**L9**	**L16**	**L9**	**L16**	**L9**	**L16 - u_x [mm]**	**HEXA elements**
1	-10.29%	-1.91%	-3.07%	-0.31%	-2.46%	4.39	0.68%
5	-13.04%	-2.08%	-3.33%	-0.30%	-2.68%	39.77	0.83%
25	-16.56%	-2.86%	-3.78%	-0.29%	-3.17%	115.37	0.75%
50	-13.66%	-3.01%	-3.32%	-0.02%	-2.96%	141.73	2.26%
100	-9.82%	-2.46%	-2.61%	0.00%	-2.18%	159.97	2.27%
500	-5.77%	-0.65%	-0.37%	-0.16%	-0.36%	210.81	1.19%
1000	-0.65%	0.11%	0.16%	-0.12%	0.23%	234.63	-
1500	-0.46%	0.06%	0.05%	-0.12%	0.18%	254.30	-
2000	-0.40%	-0.04%	-0.06%	-0.21%	0.02%	271.39	-
MAPE	-7.85%	-1.43%	-1.81%	-0.17%	-1.49%	-	1.33%
DoFs	612	1200	1044	2064	1332	2640	5085

The next analysis investigates the consistency and compatibility of various assumptions and strain measurements in a large displacements/geometric nonlinear analysis of thin-walled structures. The discretization 8b with L16 elements is used to carry out the analyses and different types of structures are considered (Fig. 12). The results of the proposed static response analysis are depicted in Fig. 13 for the geometry shown in Fig. 7, the curves of the other structures have a similar trend that not lead to additional considerations. The main differences for different structures are found in the displacement value calculated for a given

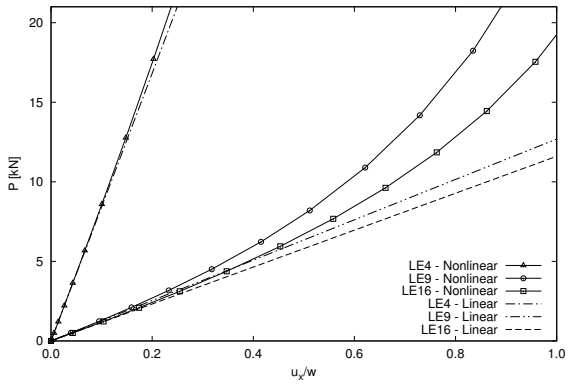

(a) Equilibrium curves of the thin-walled cross-section.

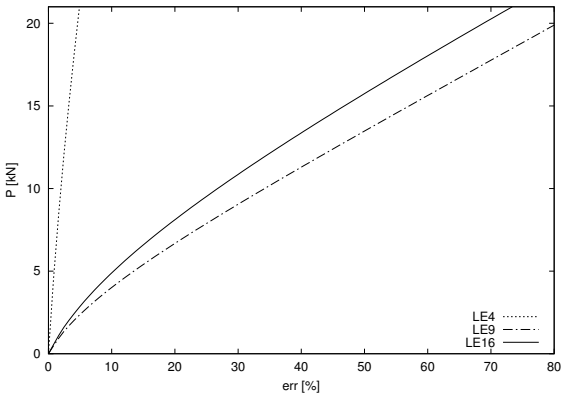

(b) Percentage difference between linear and non-linear analyses.

Figure 9: Equilibrium curve and percentage error of discretization 8a

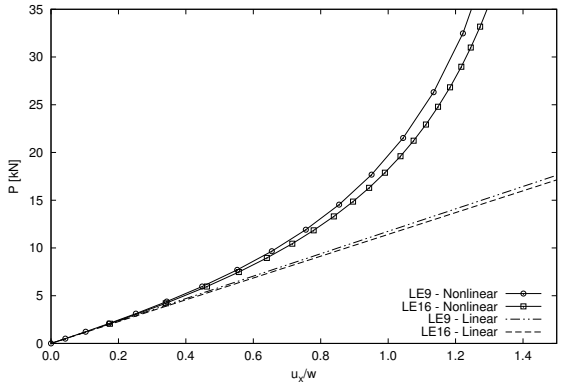

(a) Equilibrium curves of the thin-walled cross-section.

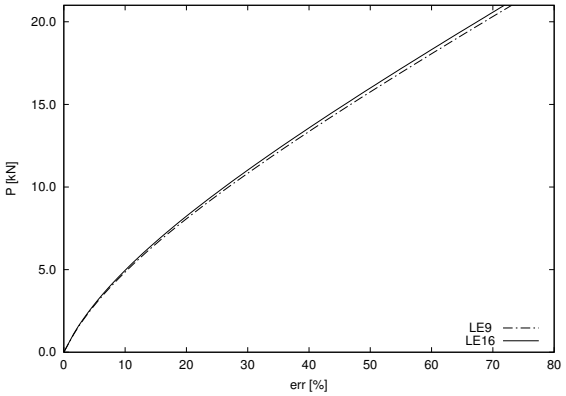

(b) Percentage difference between linear and non-linear analyses.

Figure 10: Equilibrium curve and percentage error of discretization 8b

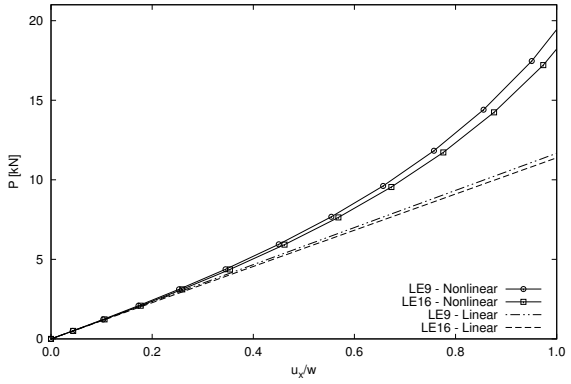

(a) Equilibrium curves of the thin-walled cross-section.

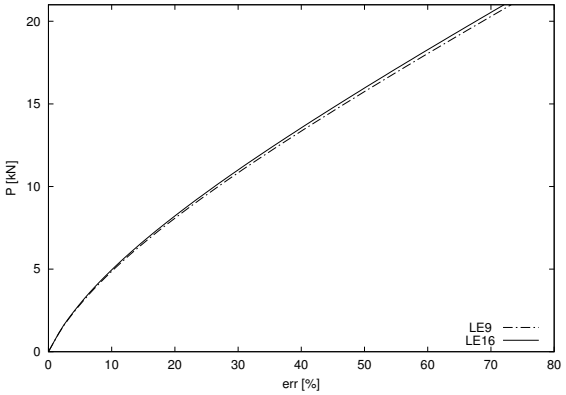

(b) Percentage difference between linear and non-linear analyses.

Figure 11: Equilibrium curve and percentage error of discretization 8c

load.

Basically, different nonlinear theories are adopted. Black dots in the matrixes in Fig. 13 denote the nonlinear terms of the matrix $\mathbf{b_{nl}}$, which are active in the correspondent analysis. The analysis marked with number 1 denotes that the nonlinearities in y-direction have no

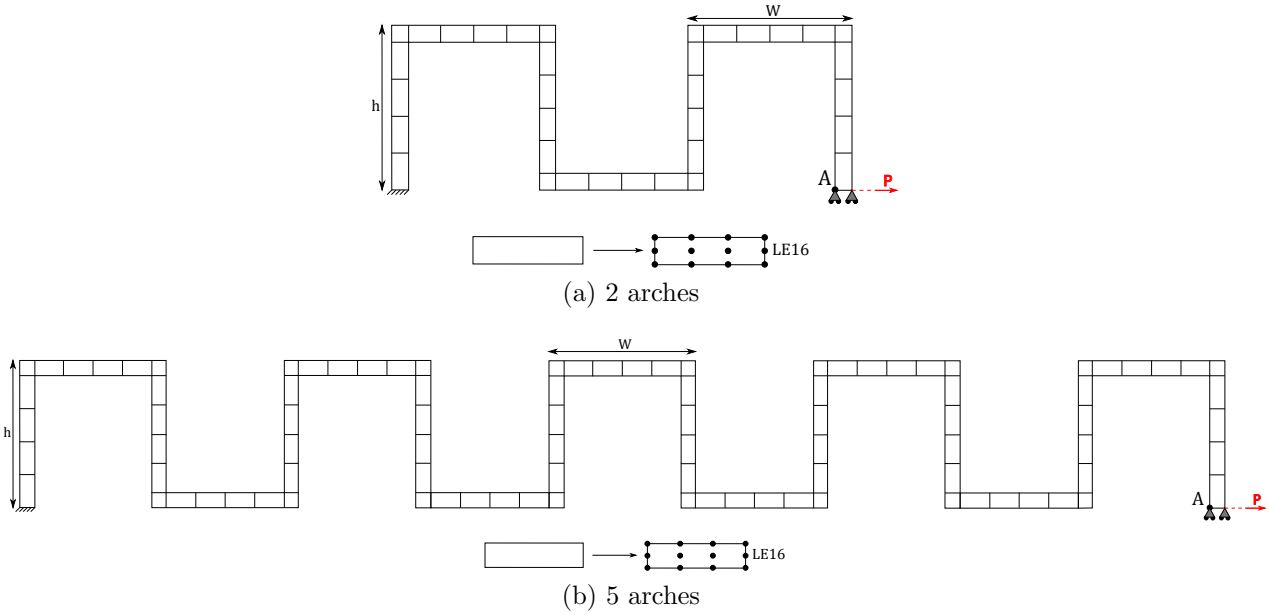

(a) 2 arches

(b) 5 arches

Figure 12: Geometry, boundary conditions and discretization cases of the thin-walled channel-section lattice structure made of multiple arches.

influence in the overall behaviour of the structure; its trend is the same compared to the nonlinear analysis where all parameters are involved. The curve 2 trend is equal to the case in which $(\partial_x \partial_z)$ terms are involved. Indeed, the shear effects have no significant impact on the behaviour of the structure. The cases from 3 to 9 show the nonlinearities in which a term of the preceding case has been neglected to find the most influential nonlinear parameters. The case 5 is almost linear until a load equal of 15 kN; at this point, the structure assumes a higher stiffness. The analysis denotes by curves 6 leads to a very different curve compared to the full nonlinear analysis. In this case, the stiffness of the beam is lower than the linear case. The comparison between the parameters demonstrates that $(\partial_x u_x)^2$ and $(\partial_z u_z)^2$ do not significantly affect the accuracy of the solution. The curves number 4 show a nonlinear analysis with only parameters $(\partial_x u_z)^2$ and $(\partial_z u_x)^2$ involved. As expected, the trend is similar to the full nonlinear analyses, and this solution is more conservative during the overall analysis. The cases 8 and 9, with only $(\partial_x u_z)^2$ or $(\partial_z u_x)^2$ involved, show a linear trend for both cases. In Fig. 14 the deformation status for three different structures are shown. In these figures can be noted that solutions, which use a reduced nonlinear matrix, can lead to results comparable with the full nonlinear case.

Increasing the overall length of the structures, the differences between a full nonlinear case and a reduced case are higher. The displacements of points A and B for different structures at P = 20 kN are listed in Table3. The shortest structures lead to lower displacement. Indeed this geometry has a higher stiffness compared to the other cases. For a point at the same coordinates (point A), the displacement is higher as the length of the structure increases. However, this increase remains constant after doubling the length of the shortest structure. The differences between a complete and a reduced case are low for the geometry shown in Fig. 7. For the others (Figs. 12a, 12b), it is more considerable. The difference between a full

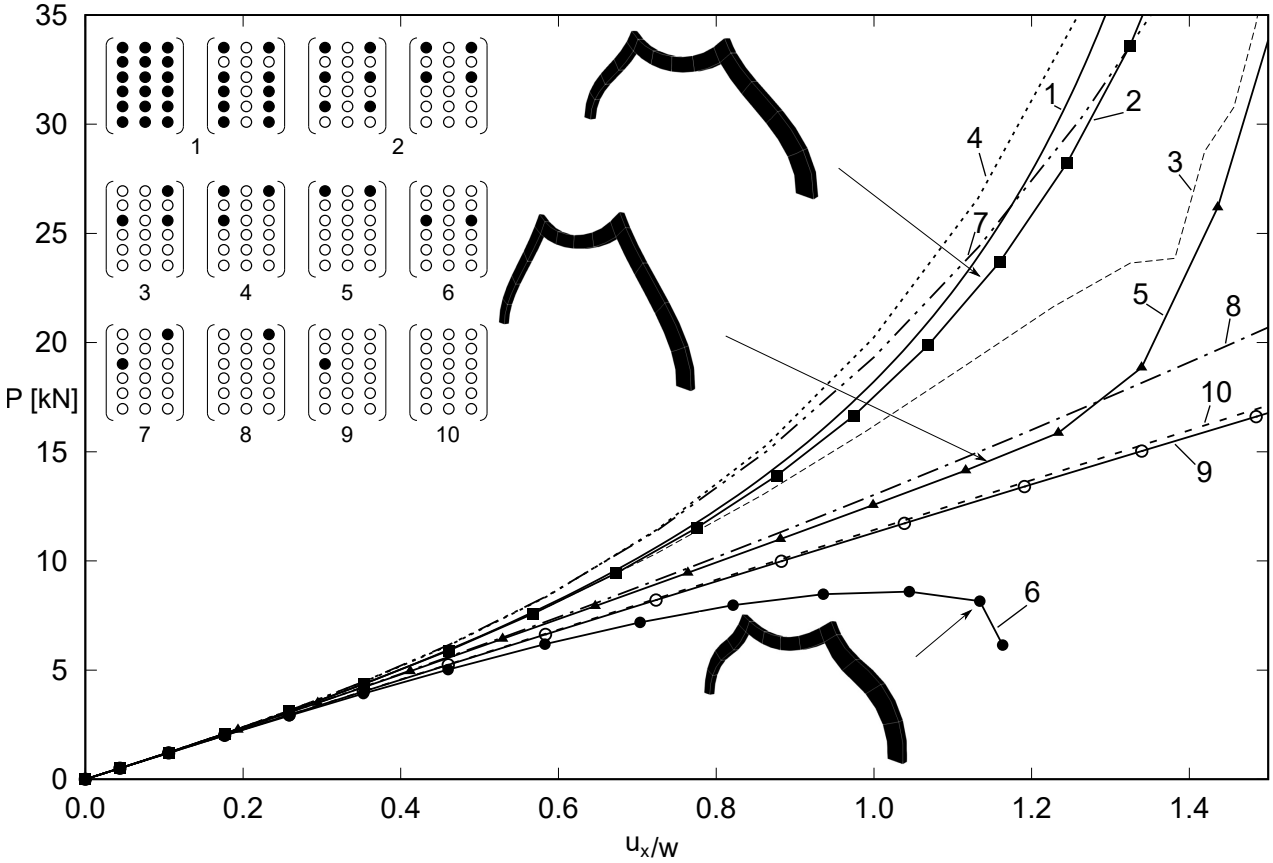

Figure 13: Equilibrium curves of the single-arch thin-walled beam for various geometrical nonlinear approximations.

Table 3: Error on displacement of point A and B for different lattice-type structures at P = 20 kN. 3D*: Nastran solution.

			3D* - HEXA	**DoFs**
A	105.32 mm	1.49 %	0.21%	CUF: 2640 3D: 5085
A	118.58 mm	3.75 %	1.13%	CUF: 4944 3D: 105342
A	118.93 mm	3.35 %	0.77%	CUF:13584 3D: 617580
B	207.82 mm	4.28 %	1.72%	-
B	535.74 mm	6.33 %	0.46%	-

and a reduced case, however, changes when considering other points in the geometry. This behaviour does not allow to establish the reliability of a set of nonlinear variables with the study of a single point of the structure. It should be noted a periodicity of the displacements for the different structures; in fact, the number of arches influence the displacement of point A. From the Table 3 it is possible to observe that the displacements of the structure with two arches and with five arches are respectively twice and five times higher of the structure with a single arch. Table 3 also shows the results obtained with 3D HEXA FEs from Nastran. Clearly, the 3D model requires more DoFs compared to the present CUF-based model, in order to catch the same displacement value.

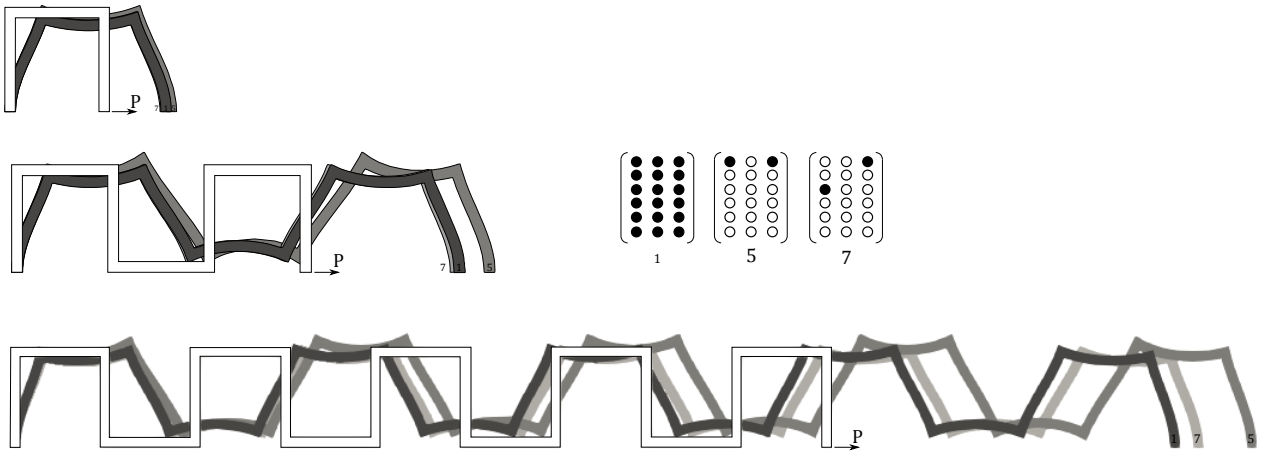

Figure 14: Deformed configurations of different lattice-type thin-walled beam for $P = 8$ kN.

In Fig. 15 the equilibrium curves for a compression load are plotted. For these analyses, the considered structure, depicted in Fig. 12b, is subjected to a compression load acting at

the same point as in the previous cases. Curves 3, 6, 7, and 9 show a hardening behaviour compared to the full case. They are characterized by the lack of the term $(\partial_x u_x)^2$, therefore not considering the variations along the x-axis leads to undersize the deformation of the structure. Curves 5 and 8 have a softening trend and they estimate a considerably higher deformation compared to the full case. Cases 2 and 4 lead to an accurate description of the behaviour of the structure, and the trends are similar to curve 1. Compared to the previous traction case, the case 7, that includes $(\partial_x u_z)^2$ and $(\partial_z u_x)^2$ terms, are not sufficient to accurately describe the nonlinear behaviour of the structure. This is mainly due to the higher length of the structure, which requires more terms of the nonlinear matrix to accurately describe its nonlinear behavior, compared to what is shown in Fig. 13. From the comparison of the curves 4 and 7, it is clear that the importance of the first term of the nonlinear matrix $(\partial_x u_x)^2$ shines. Curve 4 has the same nonlinear set as curve 7, except for the presence of the aforementioned term, and shows a more accurate solution than the one provided by curve 7. It can be concluded that for this analysis case, the derivatives along x direction, which lays along the length of the structure, takes an important role. Moreover, the set of nonlinear parameters described by curve 4 has a behaviour first hardening and then softening. Therefore it is crucial to choose the right configuration of the nonlinear matrix based on what load level the structure is analyzed.

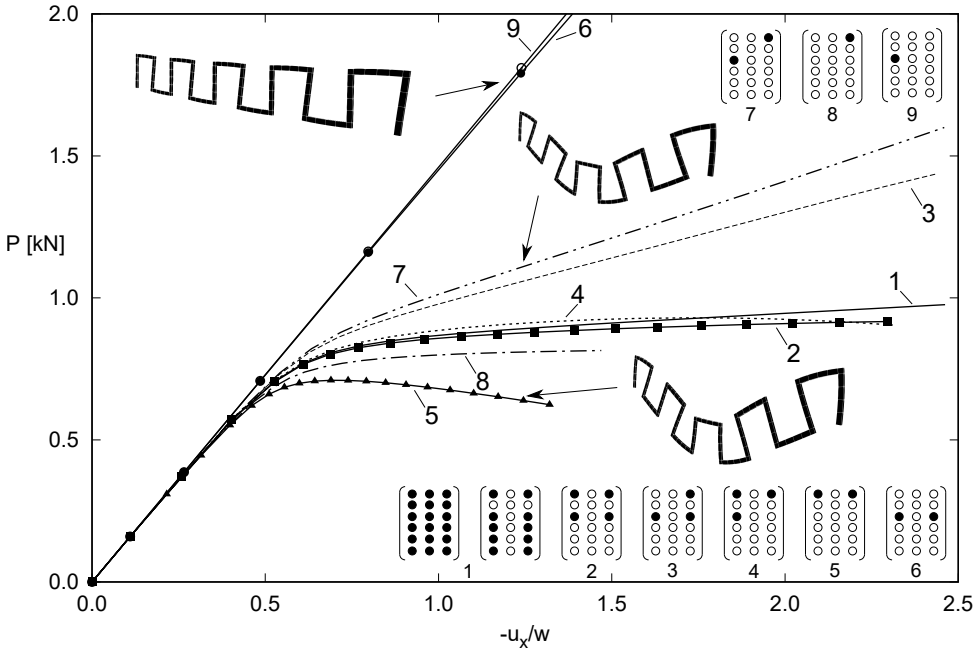

Figure 15: Equilibrium curves of the thin-walled beam for various geometrical nonlinear approximations - 5 arches.

Finally, a structure very similar to that shown in Fig. 7 is analyzed, the edges have been rounded to complicate the problem further. In Fig. 16 the geometry of the configuration with 1 or 2 arches is presented, with R = 0.03 m. The methodology presented in this paper, allows you to create a computational model by defining only the cross-section and no ad-hoc theory is needed to modelling the curved part of the structure. In Fig. 17 the equilibrium curves for different sets of parameters of the nonlinear matrix for 1 arch configuration are shown. It is interesting to note that curve 4 follows the trend of case 1 almost perfectly, adding the parameter $(\partial_z u_z)^2$ gives a greater evident error. This indicates that the different parameters have a very different influence on the nonlinear behaviour of the structure, and

the addition of one or more parameters can lead to a lower accuracy of the solution. The equilibrium curves for 2 arches configuration are shown in Fig. 18. Curve 4 represents the configuration most similar to the full nonlinear matrix case and, also in this case, the addition of the parameter $(\partial_z u_z)^2$ compromises the accuracy of the solution. By comparing the trends of curve 7 between the one and two-arch configurations (Fig. 17), it is possible to note that in this case the difference from the full nonlinear solution is higher. As already stated in the previous example, the higher is the length of the structure, the higher is the difference between the approximation of curve 7 and the full nonlinear model.

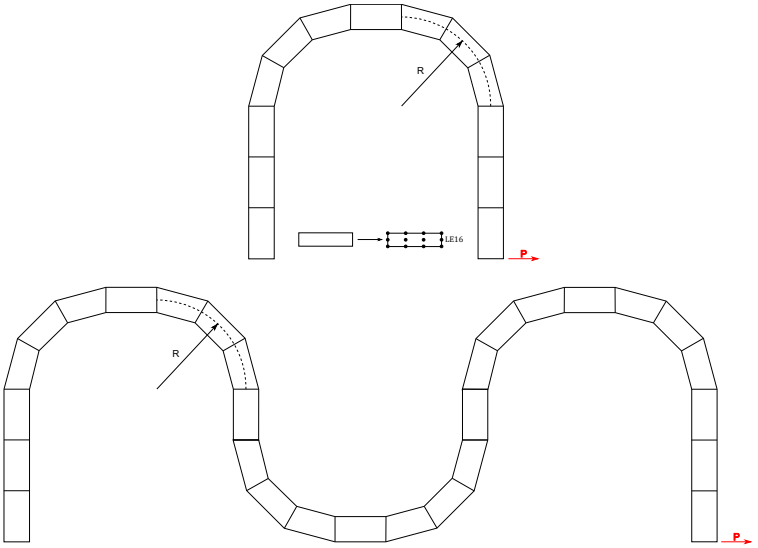

Figure 16: Geometry, boundary conditions and discretization cases of the curved thin-walled channel-section beam,

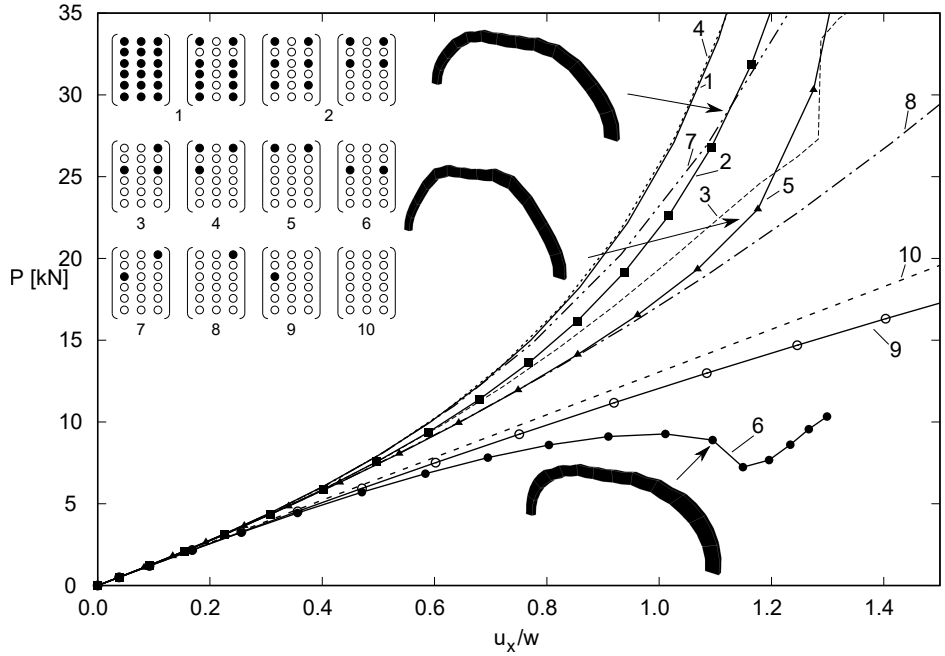

Figure 17: Equilibrium curves of the thin-walled beam for various geometrical nonlinear approximations - 1 arch curved thin-walled beam.

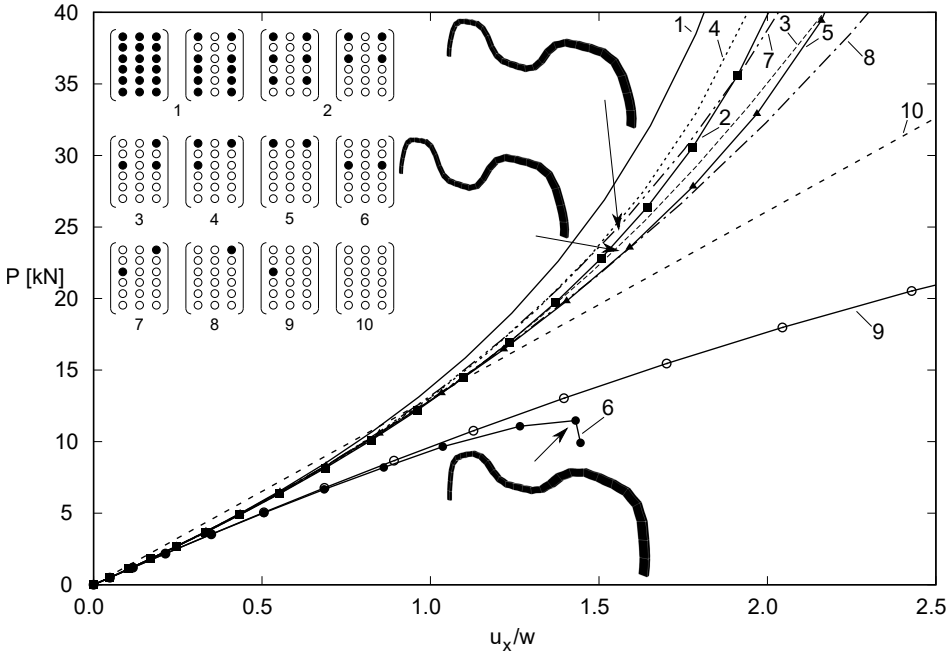

Figure 18: Equilibrium curves of the thin-walled beam for various geometrical nonlinear approximations - 2 arches curved thin-walled beam.

5 Conclusions

In this paper, various structures have been analyzed through an alternative procedure that moves most of the nonlinearities to the section nonlinearities, and, consequently, the beam axis does not play a significant role. In light of the proposed results, it is possible to draw the following conclusions:

1. The proposed methodology is able to analyze beam by leading the same accuracy of other classical approaches;

2. Such accuracy is herein obtained with a significantly lower computational cost;

3. In the proposed method, the number of Finite Elements (FEs) is significantly reduced, hence the deformations along the axis are small compared to those over the cross-section. This fact reduces the role of numerical issues, such as shear locking.

4. The accuracy and advantages of the proposed methods have been shown in both large deflection and post-buckling analysis.

5. The alternative methodology proposed herein can be used for structures with curved shapes, avoiding the use of more cumbersome strain-displacement relations in a curved reference system.

Finally, this novel approach can be adopted for solving a wide range of advanced nonlinear structural problems, including dynamic nonlinear behavior of phononic materials and metamaterials. The low computational cost of the proposed approach allows the analysis of even more complex structures, such as cross-linked latex structures, which can be made by repetitions of basic units. Furthermore, the alternative CUF approach presented in this paper can also be used to study locking buckling modes in thin-walled structures. Classical theories of obtaining local buckling due to shear distortion have some limitations that can be overcome by using the present approach.

References

[1] L. Euler. *Methodus inveniendi lineas curvas maximi minimive proprietate gaudentes sive solutio problematis isoperimetrici latissimo sensu accepti*, volume 1. Springer Science & Business Media, 1952.

[2] S. P. Timoshenko. On the transverse vibrations of bars of uniform cross-section. *The London, Edinburgh, and Dublin Philosophical Magazine and Journal of Science*, 43(253):125–131, 1922.

[3] M. De Saint-Venant. *Mémoire sur la flexion des prismes: sur les glissements transversaux et longitudinaux qui l'accompagnent lorsqu'elle ne s' opère pas uniformément ou en arc de cercle, et sur la forme courbe affectée alors par leurs sections transversales primitivement planes*. Gauthier-Villars, 1856.

[4] P. F. Pai and A. H. Nayfeh. A nonlinear composite beam theory. *Nonlinear Dynamics*, 3(4):273–303, 1992.

[5] A. W. Obst and R. K. Kapania. Nonlinear static and transient finite element analysis of laminated beams. *Composites Engineering*, 2(5-7):375–389, 1992.

[6] G. Singh, G. V. Rao, and N.G.R. Iyengar. Nonlinear bending of thin and thick unsymmetrically laminated composite beams using refined finite element model. *Computers & structures*, 42(4):471–479, 1992.

[7] K. Chandrashekhara and K. M. Bangera. Linear and geometrically non-linear analysis of composite beams under transverse loading. *Composites science and technology*, 47(4):339–347, 1993.

[8] W. Yu, D. H. Hodges, V. V. Volovoi, and E. D. Fuchs. A generalized vlasov theory for composite beams. *Thin-Walled Structures*, 43(9):1493–1511, 2005.

[9] P. Krawczyk and B. Rebora. Large deflections of laminated beams with interlayer slips. *Engineering Computations*, 2007.

[10] S. A. Emam. Analysis of shear-deformable composite beams in postbuckling. *Composite structures*, 94(1):24–30, 2011.

[11] P. Vidal and O. Polit. Assessment of the refined sinus model for the non-linear analysis of composite beams. *Composite Structures*, 87(4):370–381, 2009.

[12] Z. Li and P. Qiao. Thermal postbuckling analysis of anisotropic laminated beams with different boundary conditions resting on two-parameter elastic foundations. *European Journal of Mechanics-A/Solids*, 54:30–43, 2015.

[13] Z. Li and P. Qiao. Buckling and postbuckling behavior of shear deformable anisotropic laminated beams with initial geometric imperfections subjected to axial compression. *Engineering Structures*, 85:277–292, 2015.

[14] Z. Li and D. Yang. Thermal postbuckling analysis of anisotropic laminated beams with tubular cross-section based on higher-order theory. *Ocean Engineering*, 115:93–106, 2016.

[15] L. A. T. Mororó, A. M. C. Melo, and E. Parente Junior. Geometrically nonlinear analysis of thin-walled laminated composite beams. *Latin American Journal of Solids and Structures*, 12(11):2094–2117, 2015.

[16] Recep M Gorguluarslan, Umesh N Gandhi, Raghuram Mandapati, and Seung-Kyum Choi. Design and fabrication of periodic lattice-based cellular structures. *Computer-Aided Design and Applications*, 13(1):50–62, 2016.

[17] M. Helou and S. Kara. Design, analysis and manufacturing of lattice structures: an overview. *International Journal of Computer Integrated Manufacturing*, 31(3):243–261, 2018.

[18] K. Lee and E. Nikolaidis. A two-dimensional model for joints in vehicle structures. *Computers & structures*, 45(4):775–784, 1992.

[19] M. El-Sayed. Calculation of joint spring rates using finite element formulation. *Computers & structures*, 33(4):977–981, 1989.

[20] G.W. Jang, S. M. Choi, and Y. Y. Kim. Analysis of three thin-walled box beams connected at a joint under out-of-plane bending loads. *Journal of Engineering Mechanics*, 139(10):1350–1361, 2013.

[21] S. Donders, Y. Takahashi, R. Hadjit, T. Van Langenhove, M. Brughmans, B. Van Genechten, and W. Desmet. A reduced beam and joint concept modeling approach to optimize global vehicle body dynamics. *Finite elements in analysis and design*, 45(6-7):439–455, 2009.

[22] D. Mundo, R. Hadjit, S. Donders, M. Brughmans, P. Mas, and W. Desmet. Simplified modelling of joints and beam-like structures for biw optimization in a concept phase of the vehicle design process. *Finite Elements in Analysis and Design*, 45(6-7):456–462, 2009.

[23] E. Carrera. Theories and finite elements for multilayered, anisotropic, composite plates and shells. *Archives of Computational Methods in Engineering*, 9(2):87–140, 2002.

[24] E. Carrera, G. Giunta, and M. Petrolo. *Beam structures: classical and advanced theories*. John Wiley & Sons, 2011.

[25] A. Pagani and E. Carrera. Unified formulation of geometrically nonlinear refined beam theories. *Mechanics of Advanced Materials and Structures*, 25(1):15–31, 2018.

[26] A. Pagani and E. Carrera. Large-deflection and post-buckling analyses of laminated composite beams by carrera unified formulation. *Composite Structures*, 170:40–52, 2017.

[27] A. Pagani, E. Carrera, and R. Augello. Evaluation of various geometrical nonlinearities in the response of beams and shells. *AIAA Journal*, 57(8):3524–3533, 2019.

[28] I. Kaleel, M. Petrolo, A.M. Waas, and E. Carrera. Computationally efficient, high-fidelity micromechanics framework using refined 1d models. *Composite Structures*, 181:358–367, 2017.

[29] M. Cinefra, M. Petrolo, G. Li, and E. Carrera. Hygrothermal analysis of multilayered composite plates by variable kinematic finite elements. *Journal of Thermal Stresses*, 40(12):1502–1522, 2017.

[30] A. Entezari, M. Filippi, and E. Carrera. Unified finite element approach for generalized coupled thermoelastic analysis of 3d beam-type structures, part 1: Equations and formulation. *Journal of Thermal Stresses*, 40(11):1386–1401, 2017.

[31] M. Filippi, A. Entezari, and E. Carrera. Unified finite element approach for generalized coupled thermoelastic analysis of 3d beam-type structures, part 2: Numerical evaluations. *Journal of Thermal Stresses*, 40(11):1402–1416, 2017.

[32] E. Carrera, M. Petrolo, and P. Nali. Unified formulation applied to free vibrations finite element analysis of beams with arbitrary section. *Shock and Vibration*, 18(3):485–502, 2011.

[33] E. Carrera, A. Pagani, and R. Augello. Evaluation of geometrically nonlinear effects due to large cross-sectional deformations of compact and shell-like structures. *Mechanics of Advanced Materials and Structures*, pages 1–9, 2018.

[34] Alfonso Pagani, Ehsan Daneshkhah, Xiangyang Xu, and Erasmo Carrera. Evaluation of geometrically nonlinear terms in the large-deflection and post-buckling analysis of isotropic rectangular plates. *International Journal of Non-Linear Mechanics*, 121:103461, 2020.

[35] B Wu, A Pagani, M Filippi, WQ Chen, and E Carrera. Accurate stress fields of post-buckled laminated composite beams accounting for various kinematics. *International Journal of Non-Linear Mechanics*, 111:60–71, 2019.

[36] E. Carrera, M. Cinefra, M. Petrolo, and E. Zappino. *Finite element analysis of structures through unified formulation*. John Wiley & Sons, 2014.

[37] A. Pagani, A.G. De Miguel, M. Petrolo, and E. Carrera. Analysis of laminated beams via unified formulation and legendre polynomial expansions. *Composite Structures*, 156:78–92, 2016.

[38] E. Carrera and M. Petrolo. Refined beam elements with only displacement variables and plate/shell capabilities. *Meccanica*, 47(3):537–556, 2012.

[39] T.J.R. Hughes. *The finite element method: linear static and dynamic finite element analysis*. Courier Corporation, 2012.

[40] W. Flügge. *Stresses in shells*. Springer Science & Business Media, 2013.

[41] E Carrera, A Pagani, and R Augello. Effect of large displacements on the linearized vibration of composite beams. *International Journal of Non-Linear Mechanics*, 120:103390, 2020.

[42] E. Carrera. A study on arc-length-type methods and their operation failures illustrated by a simple model. *Computers & structures*, 50(2):217–229, 1994.

[43] M. A. Crisfield. A fast incremental/iterative solution procedure that handles "snap-through". In *Computational Methods in Nonlinear Structural and Solid Mechanics*. Elsevier, Amsterdam, Netherlands, 1981.

[44] M. A. Crisfield. An arc-length method including line searches and accelerations. *International journal for numerical methods in engineering*, 19(9):1269–1289, 1983.